SAND2016-xxxxxxx

SAND2016-2992R

Summary of available data for estimating chloride-induced SCC crack growth rates for 304/316 stainless steel

Charles Bryan and David Enos

Handout for participants in SCC Expert Panel Discussion

Sandia National Laboratories, 24-25 March, Albuquerque, NM

Sandia National Laboratories is a multi-program laboratory managed and operated by Sandia Corporation, a wholly owned subsidiary of Lockheed Martin Corporation, for the U.S. Department of Energy's National Nuclear Security Administration under contract DE-AC04-94AL85000.

1. Introduction

The majority of existing dry storage systems used for spent nuclear fuel (SNF) consist of a welded 304 stainless steel container placed within a passively-ventilated concrete or steel overpack. More recently fielded systems are constructed with dual certified 304/304L and in some cases, 316 or 316L. In service, atmospheric salts, a portion of which will be chloride bearing, will be deposited on the surface of these containers. Initially, the stainless steel canister surface temperatures will be high (exceeding the boiling point of water in many cases) due to decay heat from the SNF. As the SNF cools over time, the container surface will also cool, and deposited salts will deliquesce to form potentially corrosive chloride-rich brines. Because austenitic stainless steels are prone to chloride-induced stress corrosion cracking (CISCC), the concern has been raised that SCC may significantly impact long-term canister performance. While the susceptibility of austenitic stainless steels to CISCC in the general sense is well known, the behavior of SCC cracks (i.e., initiation and propagation behavior) under the aforementioned atmospheric conditions is poorly understood.

A literature survey has been performed to identify SCC crack growth rate (CGR) studies conducted utilizing conditions that may be relevant to existing SNF interim storage canisters, the results of which are presented in this document. The data presented here have been restricted to those representing atmospheric corrosion of stainless steels due to deliquescence of marine salts, or marine salt components, on the metal surface. A suite of experimental studies representing both long-term field tests and accelerated laboratory tests has been identified. Potentially relevant data are summarized in Figures 1-1 (304 SS) and Figure 1-2 (316 SS). In the Figures, when a particular reference utilized a series of samples, the range is shown as a bar, and the average value shown with a symbol. A summary of the test methods, sample geometry, and environmental conditions for each study is given in Table 1-1.

While the surveyed studies all explore SCC of austenitic stainless steels under atmospheric conditions, the methods through which each researcher approached the problem do differ, as illustrated in Table 1-1. The surveyed studies utilized a variety of metal treatments including as-fabricated, solution annealed, welded, and sensitized material. Furthermore, different surface treatments (polished vs ground) were also used. In addition, most of these studies were accomplished using techniques that are not generally accepted for high-fidelity crack growth rate measurements, and in cases where more traditional approaches were taken, these methodologies may not be applicable to the atmospheric conditions of interest here. The wide variety of methods and materials results in the observed large scatter in measured CGRs. Each of the data sets in Figures 1-1 and 1-2 is described in more detail in the following sections. A short summary of crack growth rates based on operational experience is also presented.

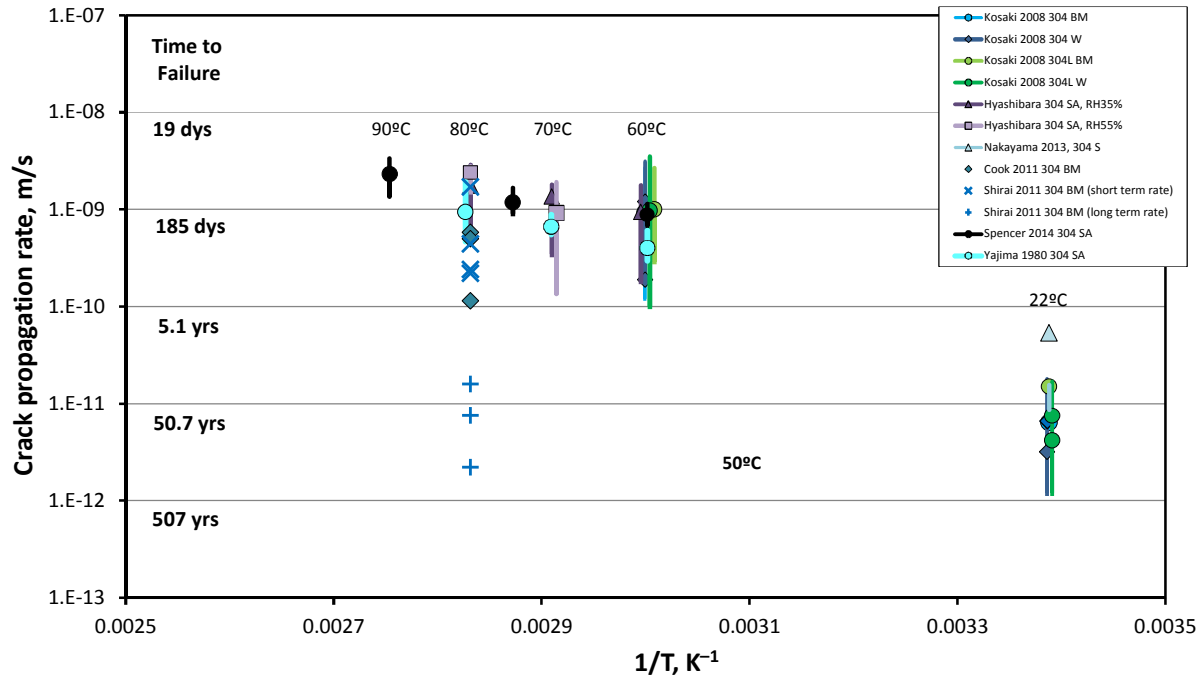

Figure 1-1. SCC propagation rates for atmospheric corrosion of 304SS. BM –base metal; W–weld sample; SA–solution annealed; S–sensitized. Bars represent reported ranges (if more than one), while symbols represent average values. "Times to failure" are for a 5/8" thickness, assuming continuous crack propagation over time.

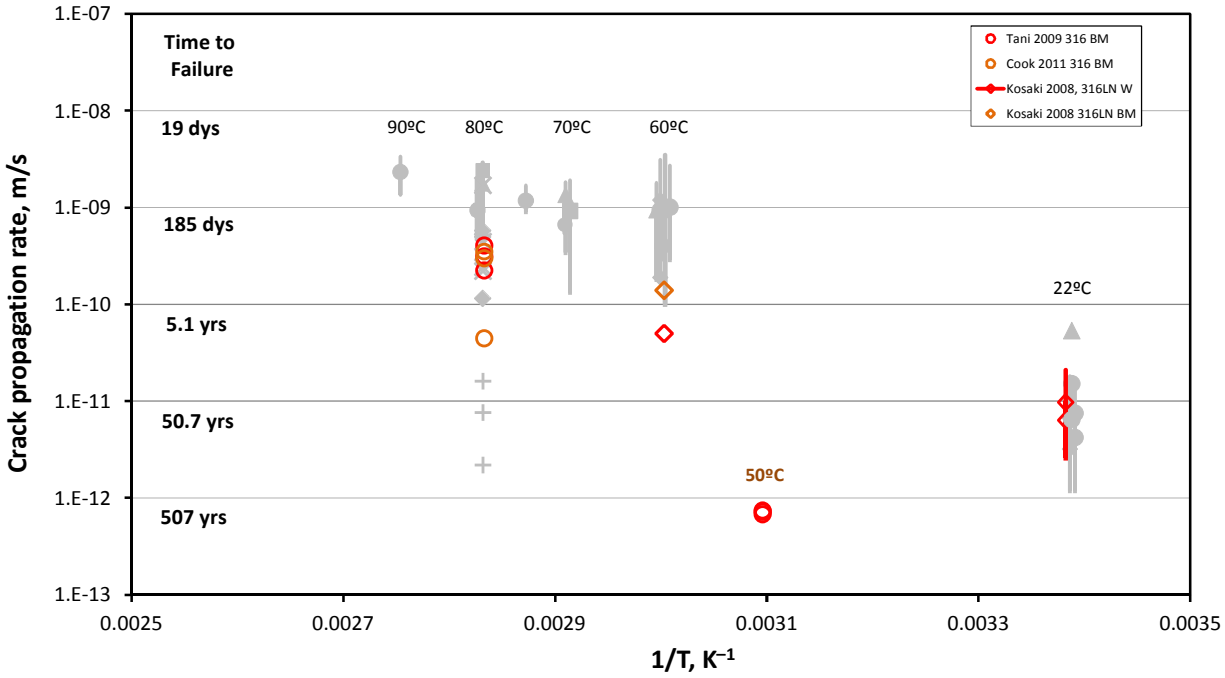

Figure 1-2. SCC propagation rates for atmospheric corrosion of 316SS. "Times to failure" are for a 5/8" thickness, assuming continuous crack propagation over time.

Table 1: Summary of SCC Crack Growth Rate Studies

Researcher		Materials	Salt Loading Method	Environments	Sample Geometry	Crack Geometry	CGR Measurement method
Kosaki	2008	304, 304L, 316LNG	1. Natural exposure 2. Salt fog (saturated NaCl)	1. Ambient 2. 60C/95% RH	Initiation: 4 point bent Propagation: 3 point bend	Fatigue precrack described as through crack and half-elliptical surface crack	Optical - max depth/time
Hayashibara	2008	304 (solution annealed)	10 uL droplet of seawater placed on samples	35-75% RH, 60-90C	Dogbone, spring loaded	no precrack, nucleation from localized corrosion sites Final geometry not described	Length measured in SEM, depth optically
Nakayama	2013	304, 304H	natural exposure	ambient	U-bend	no precrack, nucleation from localized corrosion sites	Optical - surface length measured, depth calculated
Cook	2011	304L, 316L	coated with sea salt or $MgCl_2$ applied as a mist then dried	32% RH, 80C	U-bend	no precrack, nucleation from localized corrosion sites	Optical - surface length measured, depth calculated
Spencer	2014	304L, cold worked	$MgCl_2$ applied via air brush with an EtOH carrier. Deposit weight not measured	60-90C, 10-70% RH	Bend bar	no precrack, nucleation from localized corrosion sites Crack length on surface measured	Optical - surface length measured. Rate = length/time
Tani	2009	316L, 312	synthetic seawater droplet injected into notch	80C, 35% RH	CT specimen	Crack geometry not presented upon completion of test	DCPD
Shirai Tani	2011 2010	304L	$MgCl_2$ droplet or possibly spray	80C, 35% RH	4 point bend bar	no precrack - nucleation from localized corrosion site	DCPD

2. Available Data on Atmospheric SCC Crack Growth Rates

2.1 *Kosaki* [2008]

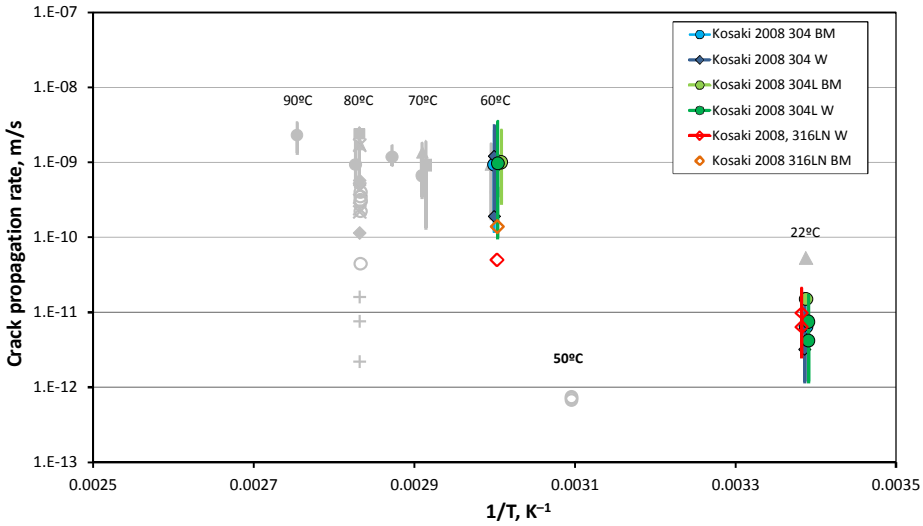

Figure 2.1-1. Data from *Kosaki* [2008].

Kosaki [2008] evaluated performance of stainless steels, including 304, 304L, 316LN, and both base-metal and welded specimens were used. Corrosion rates were measured in long-term natural exposure tests in a near-marine setting (Miyakojima Island south of Okinawa; tropical rainforest to humid subtropical climate); both exposed samples and under-glass samples (to avoid rain washing) were used. An accelerated test was also run (60ºC, 95% RH, NaCl "steam"). Both crack initiation and crack growth experiments were run.

The crack initiation experiments were run using 4-point bend specimens at tensile stresses of 0.5 and 1.0 σ_y. At ambient conditions, exposed and under glass, SCC crack initiation was observed only of the 304 weld specimens, over the ~2.5 year duration of the test. Under accelerated conditions, SCC cracking was observed within 30 days for all samples.

Crack growth experiments were done with 3-point bend specimens, with applied outer fiber stresses of 0.4 and 0.8 σ_y. Pre-cracks were induced by fatiguing (thermal?) and are described as "*…through crack and half-elliptical surface crack…*" It is not clear what "*through crack*" means, but the diagram in the paper (see Figure 2.1-2), seems to show a vertical crack penetrating the sample (with crack propagation rates measured as lateral growth?). SCC crack growth rates were measured by fully fracturing the samples and performing post-mortem visual analysis (reported CGRs were calculated ignoring incubation time, and are hence minimum values). While SCC initiation was rarely observed in the initiation experiment, SCC crack growth was measured in

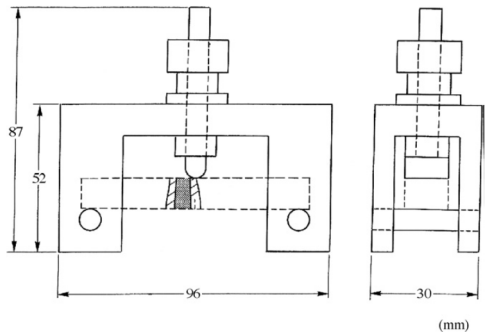

Figure 2.1-2. 3-point bending specimen for SCC propagation test [*Kosaki* 2008, Figure 5].

most of the pre-cracked CGR test samples. Results are summarized in Table 2.1-1 [*Kosaki* 2008, Table 2]. There was little difference between weld and base metal samples for 304 and 304L, and little difference in measured rates for those two materials. The 316LN performed better, with no observed SCC in the unwelded samples at ambient conditions, and slightly slower corrosion rates in the accelerated test. Perhaps surprisingly, the under-glass specimens performed significantly better than the exposed specimens.

Table 2.1-1. Propagation rates of SCC in test materials [*Kosaki* 2008, Table 2]

Material	SCC propagation rate, natural exposure (m/s)		SCC propagation rate, accelerated test (m/s)
	Direct exposure A1	Under glass exposure A2	
Type 304			
Base metal	6.4E−12	(no SCC)	9.3E−10 (1.2E−10 to 2.7E−9)
Weld	6.6E−12 (2.1E−12 to 1.8E−11)	3.2E−12 (1.2E−12 to 6.4E−12)	1.2E−09 (1.9E−10 to 3.1E−9)
Type 304L			
Base metal	1.5E−11	(no SCC)	1.0E−09 (2.9E−10 to 2.7E−9)
Weld	7.5E−12 (1.2E−12 to 1.7E−11)	4.2E−12 (4.1E−12, 4.3E−12)	9.7E−10 (1.0E−10 to 3.5E−9)
Type 316LN			
Base metal	(no SCC)	(no SCC)	1.4E−10
Weld	9.8E−12 (2.6E−12 to 2.1E−11)	6.4E−12	5.0E−11

Note: Propagation rates of SCC show average values and values in ( ) show scattering range of data.

Raw data are shown in Figure 2.1-3 [*Kosaki* 2008, Figures 5 and 6]. The authors report no CGR dependence on stress intensity factor (K_I) over a range of 0.5 to 30 MPa. However, for the stated experimental design—three-point bend specimens with a fixed load and with pre-cracks of different geometries---it seems impossible to actually calculate an accurate K_I value, or to achieve the range described. For instance, for an elliptical crack, at the cited applied stresses, the CGR would have to be measured at a depth of 10 microns to obtain a rate at $K_I = 0.5$ MPa $m^{½}$. Conversely, actually achieving a measurable or calculable K_I of 30 MPa $m^{½}$ would be very difficult in a sample of the cited dimensions (90 mm long × 15 mm wide × 10 mm thick). For either of the proposed pre-crack geometries, it is not clear how K_I values could have been accurately estimated at any point along the crack front.

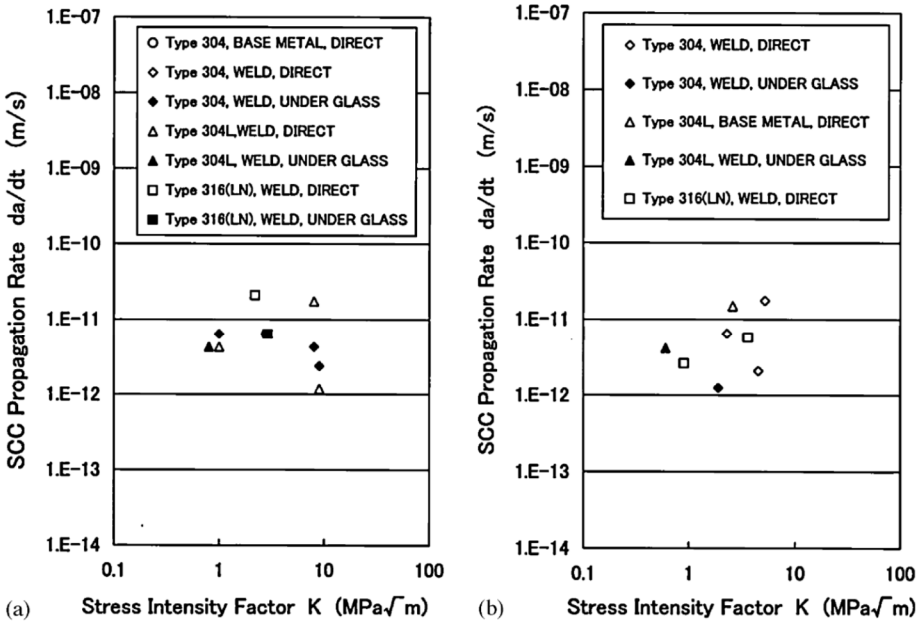

Fig. 6. SCC propagation rate of Type 304 (natural exposure test). (a) Penetrate pre-crack; (b) half elliptical surface pre-crack.

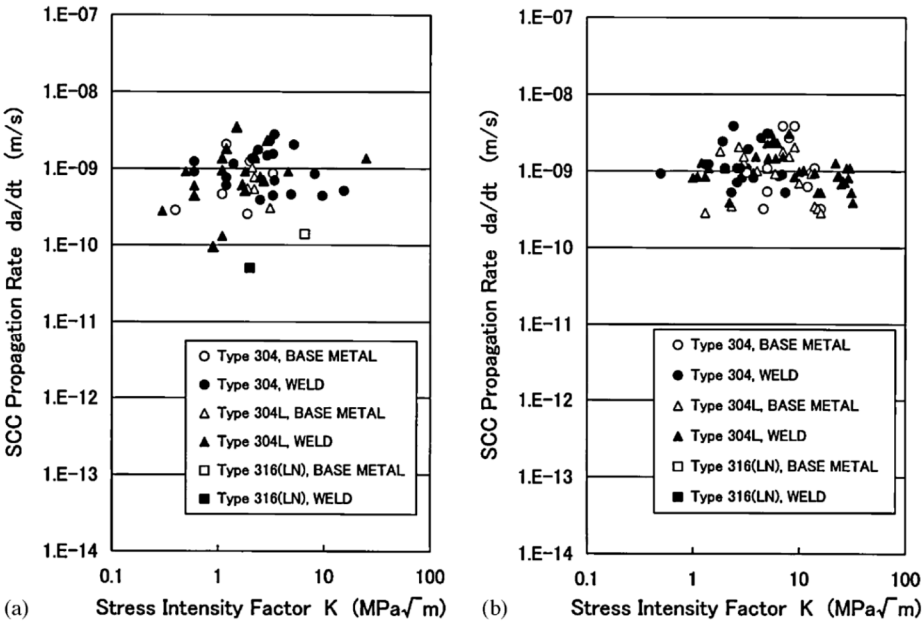

Fig. 7. SCC propagation rate of Type 304 (accelerated test). (a) Penetrate pre-crack; (b) half elliptical surface pre-crack.

Figure 2.1-3. CGR data as a function of K_I from *Kosaki* [2008, Figures 6 and 7].

2.2 *Hayashibara et al.* [2008]

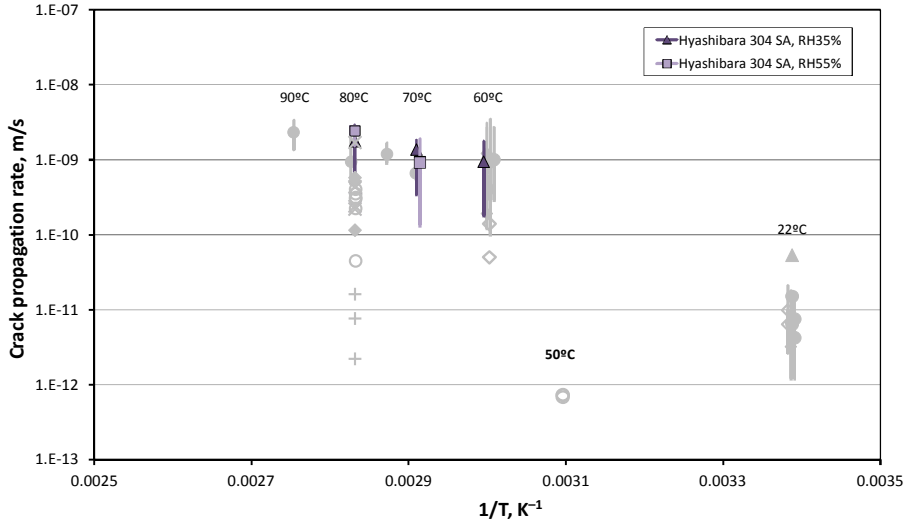

Figure 2.2-1. Data from *Hayashibara et al.* [2008]

This laboratory study was carried out using solution-annealed 304 stainless steel under constant load uniaxial tensile stresses of 0.5 to 1.25 $\sigma_{0.2}$ (reported to be 313 MPa at room temperature). Specimens were dogbone-type specimens, 100 mm long and 26 mm wide with an 8 mm gauge section, and 2 mm thick. Specimens were held at temperatures of 80ºC, 70ºC, and 60ºC, at RH values of 35%, 55%, and 75% for 120 to 1075 hours. Samples were loaded with salt by applying 10µL droplets of synthetic seawater onto three points of the metal surface within the gauge section. Crack lengths were measured optically after conclusion of the experiment (reported CGRs were calculated ignoring any incubation time, and are hence minimum values). CGRs as a function of applied tensile stress from *Hayashibara et al.* [2008] are shown in Figure 2.2-2 and Figure 2.2-3. At 80ºC, the maximum growth rate did not depend on applied stress, but at 70ºC and 60ºC, the crack growth rate increased with increasing tensile stress. SCC initiation strongly depended on RH at all temperatures. At 55% RH, SCC initiated at all chloride spots, while at 35% RH, SCC initiated at all applied stresses, but a much higher fraction of chloride spots initiated at tensile stresses equal to $\sigma_{0.2}$ or higher. Measured crack growth rates were highly scattered, and the range of possible activation energies was estimated to be 23–105 kJ mol^{-1}. The authors suggested that the scatter was due to differences in crack incubation time with temperature, and proposed that the lower end of this range, from 23 to 39 kJ mol^{-1} (based on the highest crack rates, which were likely the first to initiate and hence the most likely to not include a significant incubation time) were preferred.

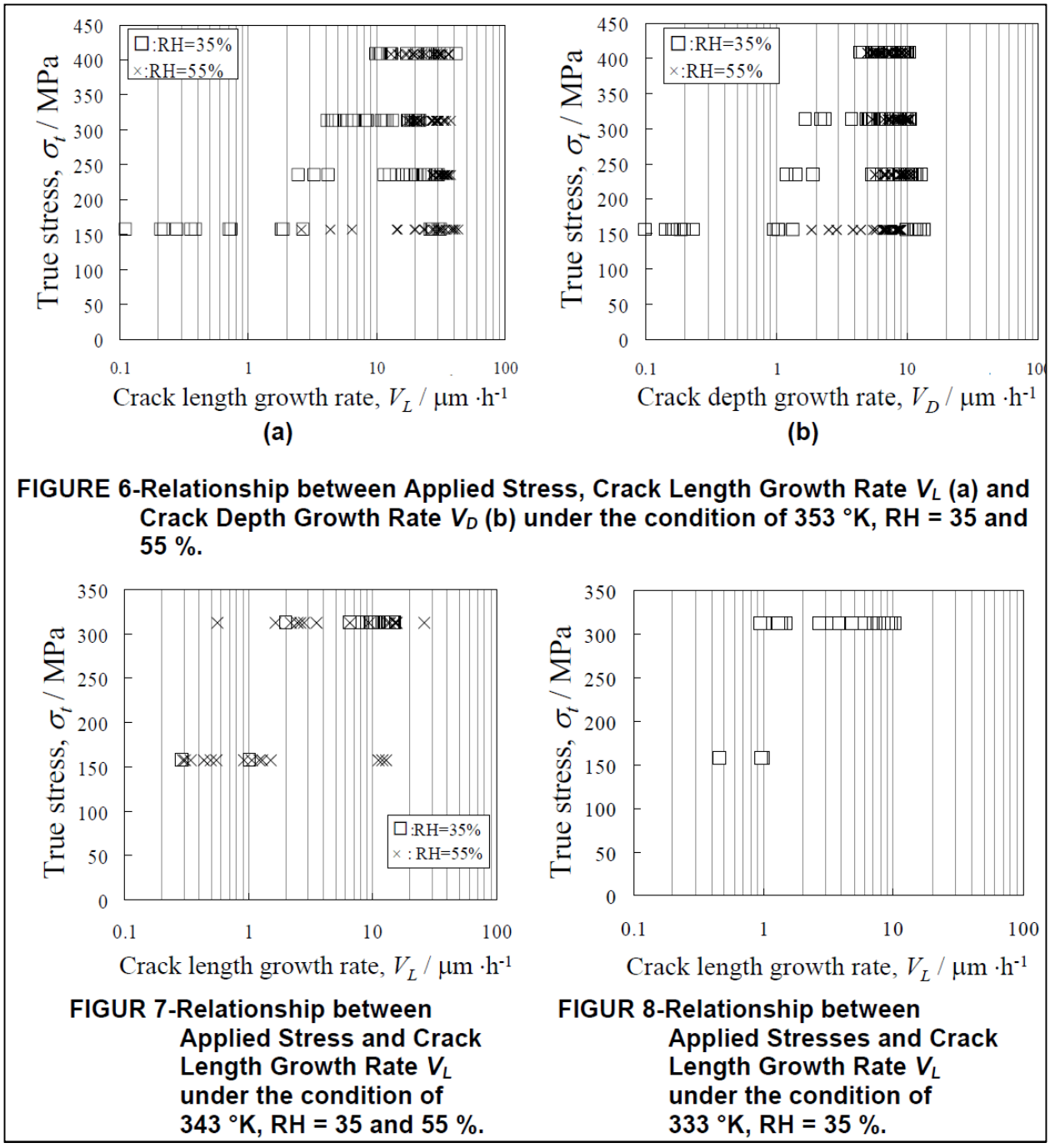

FIGURE 6-Relationship between Applied Stress, Crack Length Growth Rate V_L (a) and Crack Depth Growth Rate V_D (b) under the condition of 353 °K, RH = 35 and 55 %.

FIGUR 7-Relationship between Applied Stress and Crack Length Growth Rate V_L under the condition of 343 °K, RH = 35 and 55 %.

FIGUR 8-Relationship between Applied Stresses and Crack Length Growth Rate V_L under the condition of 333 °K, RH = 35 %.

Figure 2.2-2. CGR data for both crack length and crack depth, as a function of applied tensile stress. Data from *Hayashibara et al.* [2008; Figures 6-8].

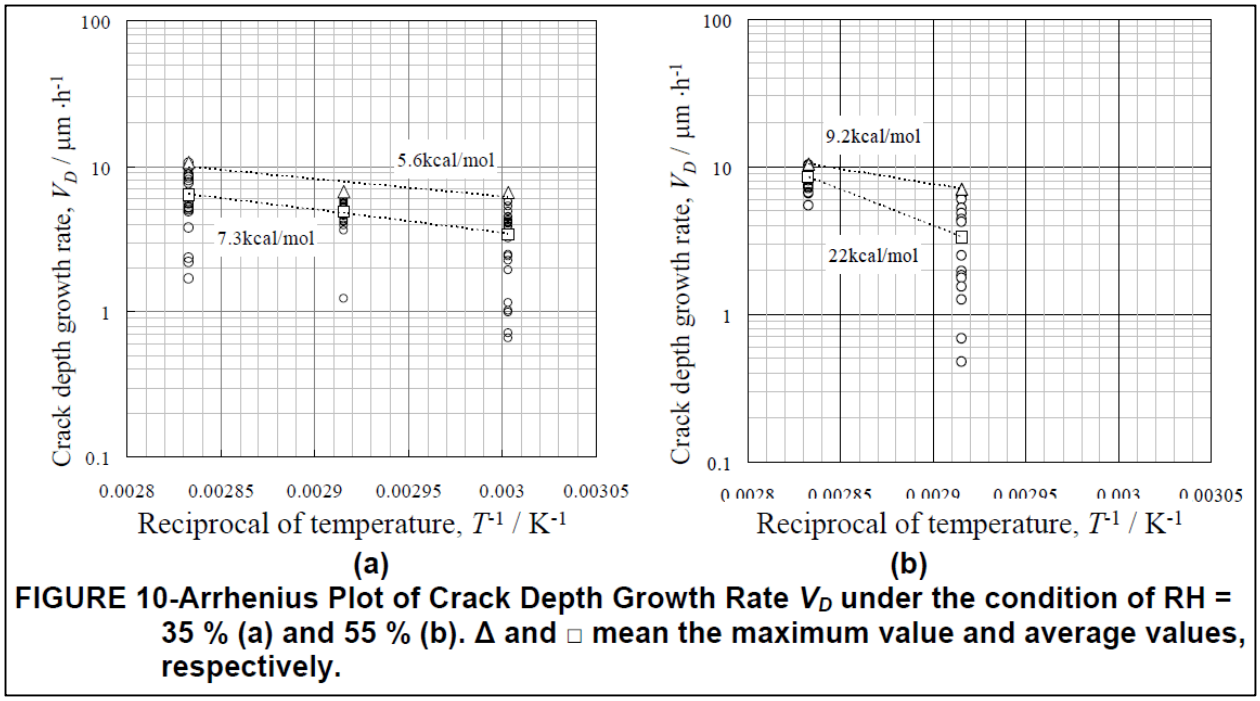

FIGURE 10-Arrhenius Plot of Crack Depth Growth Rate V_D under the condition of RH = 35 % (a) and 55 % (b). Δ and □ mean the maximum value and average values, respectively.

Figure 2.2-3. Arrhenius plots for crack depth CGR data from *Hayashibara et al.* [2008; Figure 10].

2.3 *Nakayama and Sakakibara* [2013]

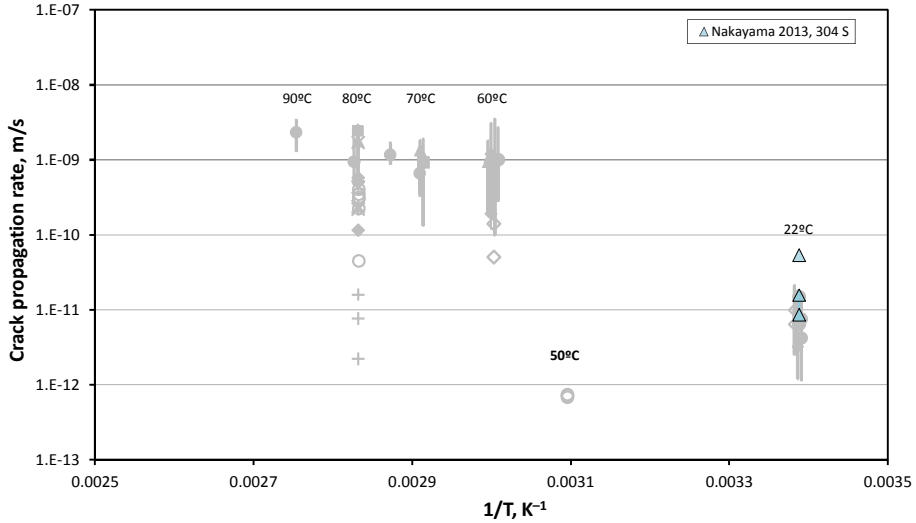

Figure 2.3-1. Data from *Nakayama and Sakakibara* [2013].

This article summarized test data collected in Japan that is published in several Japanese-language reports. The authors used the data to build a time-to-failure model for repair-welded joints, for 304 SS canisters with wall thicknesses of 20 mm.

The testing work used 304 stainless steel U-bend specimens sensitized to R_a values of 2% to 20%, and demonstrated that SCC initiation and propagation rates, over the interval of the test, were strongly a function of R_a. One set of samples was exposed to marine salts at a shipyard (both without a roof and under a roof), while a second set was placed at an inland site. The exposed near-marine samples cracked within half a year, with crack length growth rates of 0.54 – 3.36 mm yr^{-1}; the under-roof near-marine samples initiated SCC more slowly, but once initiated (0.8 yrs), grew quickly at 0.99 mm yr^{-1}. The crack depth data in Figure 8 were calculated by assuming a crack depth-to-half-surface-length ratio of 0.5—the range of 0.3 to 0.5 is typical for austenitic materials (Lu et al., 2005). The authors present other data showing strong crack growth rate dependencies on R_a, $[Cl^-]$, m_{Cl} on the surface, and applied stress, and present a SCC initiation and growth models incorporating all of these.

2.4 *Cook et al.* [2011]

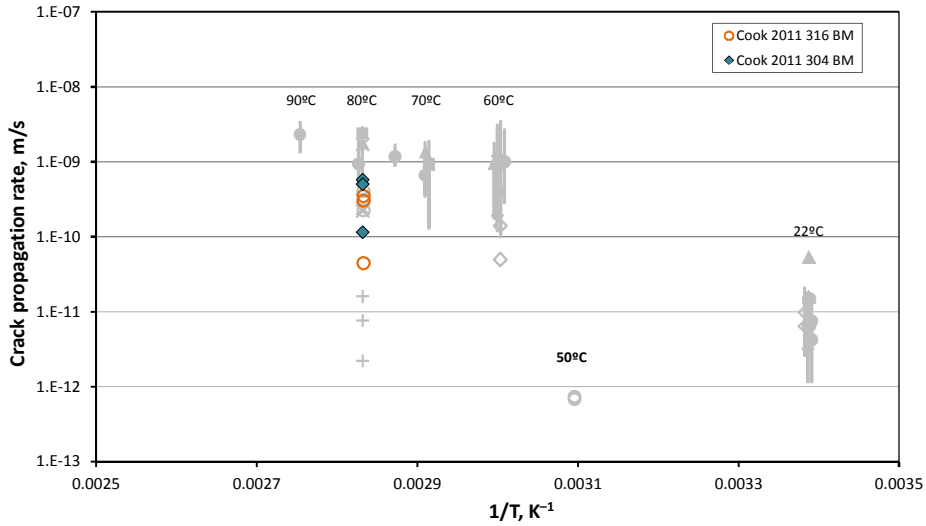

Figure 2.4-1. Data from *Cook et al.* [2011].

Cook et al. [2011] evaluated SCC of both 304L SS and 316L SS U-bend samples (applied stresses not provided) coated with sea-salts and with magnesium chloride in laboratory tests at a temperature of 80ºC and a RH of 30% (conditions not possible on a canister surface). Corrosion was measured after 42 days of exposure. SCC crack lengths were measured and reported in the reference; the crack depth data in Figure 2.4-1 were calculated from those data by assuming a crack depth-to-half-surface-length ratio of 0.5—the range of 0.3 to 0.5 is typical for austenitic materials [*Lu et al.*, 2005]. CGRs were calculated from the total exposure time (no incubation time) and hence are minimums.

2.5 *Spencer et al.* (2014)

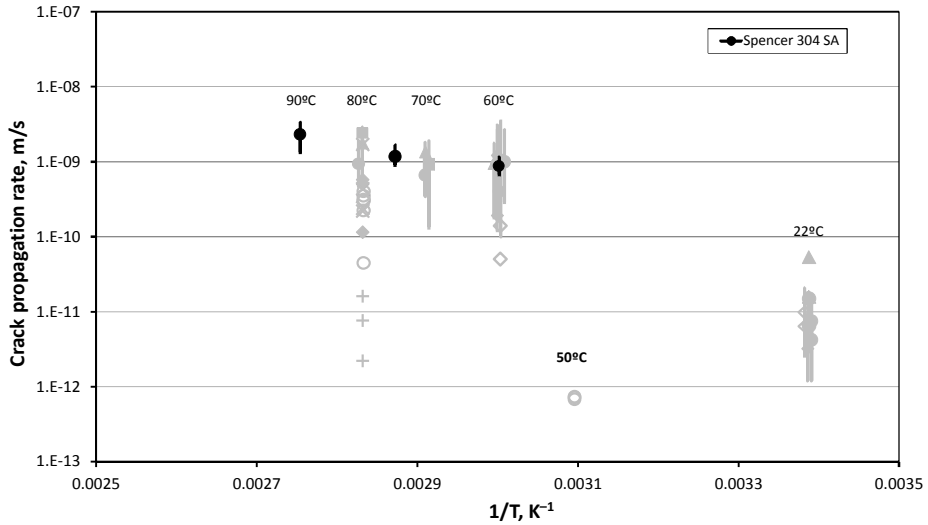

Figure 2.5-1. Data from *Spencer et al.* [2014].

Spencer et al. [2014] performed laboratory tests evaluating SCC crack growth rates in annealed 304L ($\sigma_{0.2}$ was 210 MPa after annealing), and to which a uniaxial plastic strain had been applied (the authors were evaluating, in part, the importance of prior plastic strain on SCC initiation and growth). A spring-loaded bend geometry was used for the CGR tests (Figure 2.5-2). Samples were loaded with a visible coating magnesium chloride, applied as a methanol spray and allowed to dry. Surface loading was not measured.

Tests were run at 60º, 75º, and 90ºC, and saturated salt solutions were used to maintain constant relative humidities in the test chambers, at values varying from 10% to 70%. Plastic strains varied from 0 -40%, and tensile stresses (outer fiber) up to 180 MPa. Test results showed a strong dependence on the degree of prior plastic strain, with maximum CGR at values of less than 10% strain; at higher strains, cracking did not occur (Figure 2.5-3). Although here appeared to be a threshold tensile stress of about 10 MPa, crack parameters (maximum and average growth rate, and crack density) rose quickly with increasing stress and plateaued rapidly. Cracking was not observed at 10 % RH, the lowest value tested, but was observed at 30% RH and above, for tensile stresses of both 60 MPa and 120 MPa. CGRs showed a general increase with RH, but the overall response to variation in RH varied with tensile stress and degree of prior strain (Figure 2.5-4).

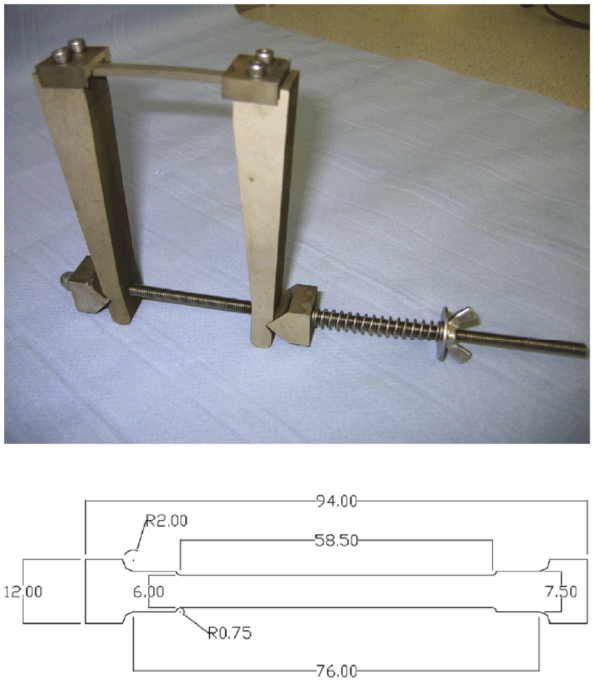

Figure 2.5-2. Bend test assembly used in *Spencer et al.* [2014, Figure 1].

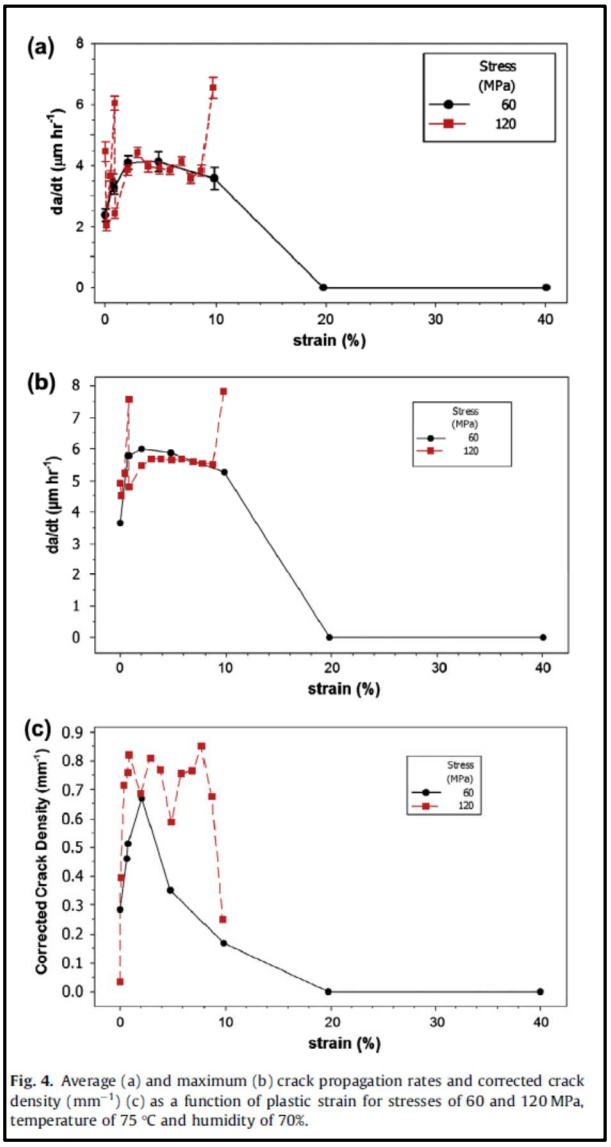

Fig. 4. Average (a) and maximum (b) crack propagation rates and corrected crack density (mm^{-1}) (c) as a function of plastic strain for stresses of 60 and 120 MPa, temperature of 75 °C and humidity of 70%.

Figure 2.5-3. Measured crack parameters as a function of degree of prior plastic strain. Data from *Spencer et al.* [2014; Figure 4].

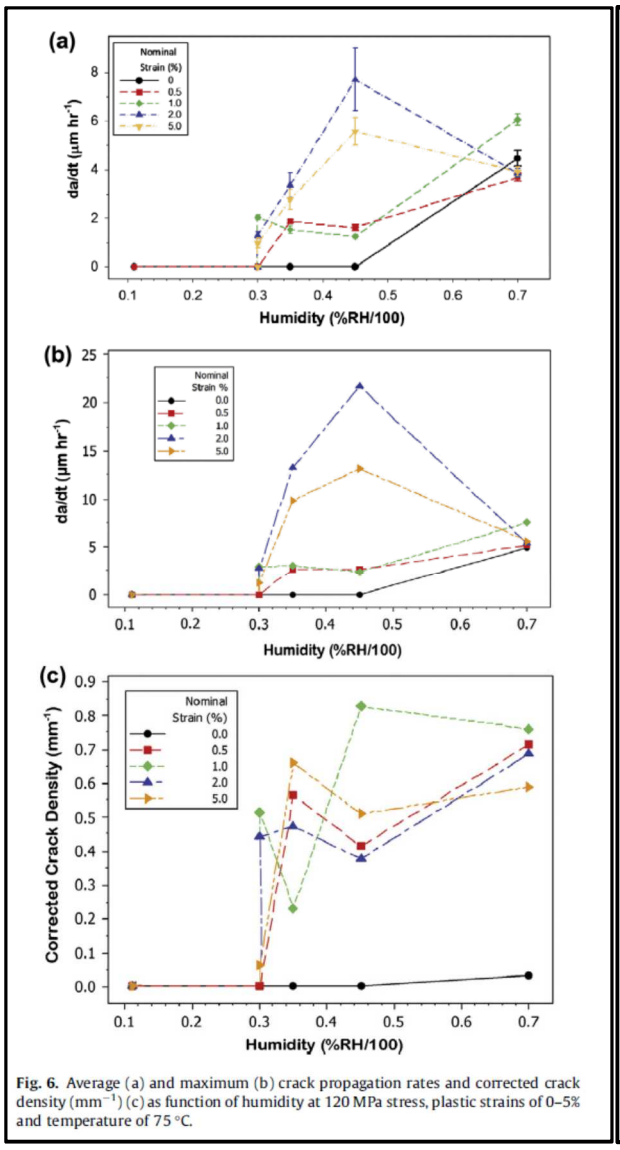

Fig. 6. Average (a) and maximum (b) crack propagation rates and corrected crack density (mm^{-1}) (c) as function of humidity at 120 MPa stress, plastic strains of 0–5% and temperature of 75 °C.

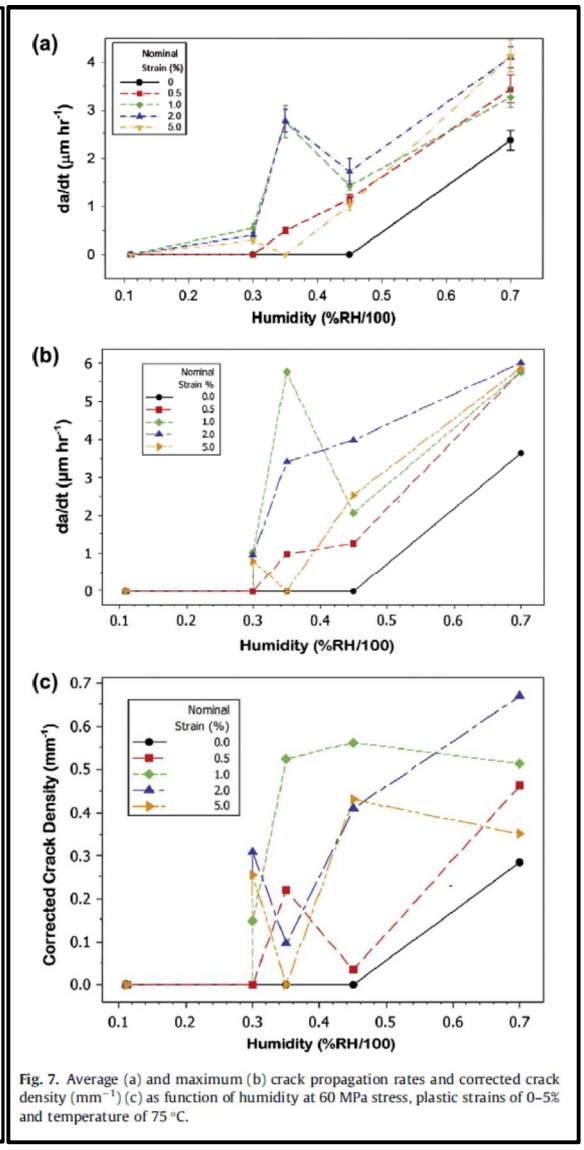

Fig. 7. Average (a) and maximum (b) crack propagation rates and corrected crack density (mm^{-1}) (c) as function of humidity at 60 MPa stress, plastic strains of 0–5% and temperature of 75 °C.

Figure 2.5-4. *Spencer et al.* [2014; Figures 6 and 7]; measured crack parameters as a function of relative humidity, for tensile stresses of (left) 120 MPs, and (right) 60 MPa.

Measured CRGs reported by *Spencer et al.* [2014], for samples with 2-5% plastic strain at 70% RH, were 8.9±3 µm/hr (2.5E-9 m/s) at 90ºC; 4.2±0.956 (1.2E-9 m/s) at 75ºC; and 3.2±0.64 µm/hr (8.9E-10 m/s) at 60ºC. Spencer used these samples to estimate an apparent activation energy of 33.7 kJ mol^{-1}.

2.6 Data from CRIEPI

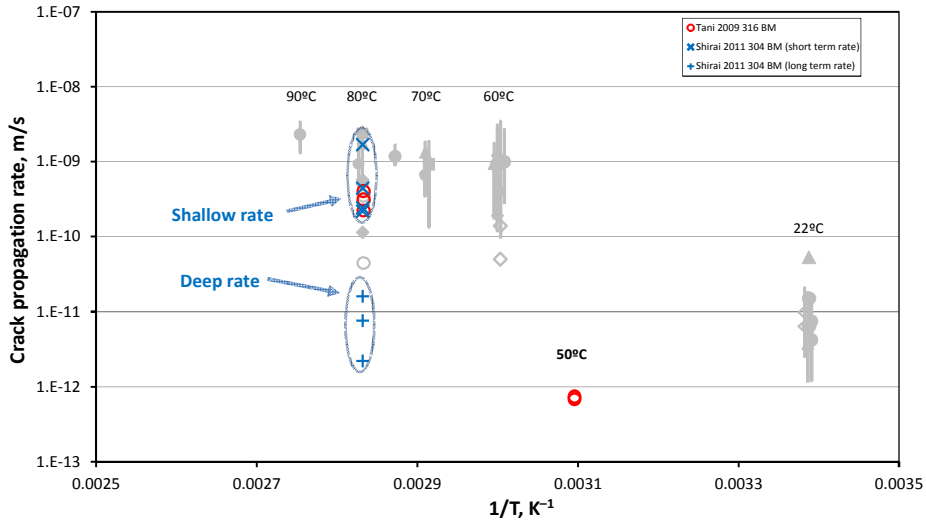

Figure 2.6-1. Data from CRIEPI.

The Central Research Institute of Electric Power Industry (CRIEPI), a research institute of the Japanese nuclear industry, ran two types of experiments evaluating CGR under atmospheric conditions. In the first [*Tani et al.*, 2009], compact tension tests were run with 316 SS, loaded to achieve K values of 5–30 MPa $m^{0.5}$. Samples were loaded with salt by applying 20µL droplets of synthetic seawater directly to the CT notch. Tests were run at 50ºC and 80ºC, at a constant RH of 35% for the duration of the test. Crack depths were determined by DCPD. At stress intensity factors of 10 MPa $m^{0.5}$ and above, there was no variation in crack growth rate with applied stress; the single 80ºC test at 5 MPa $m^{0.5}$ was about 60 times lower than the 80ºC tests at higher K values (note that this point is not shown above, as it was apparently not a "plateau" value, and is not directly relatable to the other data.

The second type of experiment that CRIEPI ran were four-point bend tests [*Shirai et al.*, 2011a; *Shirai et al.*, 2011b; *Shirai et al.*, 2011c; *Tani et al.*, 2010]. The beams used for these tests were 20 mm wide, 10 mm thick, and 220 mm long. These tests were run using 304SS, at 80ºC and 35% RH (conditions corresponding to an absolute humidity to high to be achieved on a canister surface), with an applied outer fiber tensile stress of 270 MPa. The specimens used are quite thick, so that crack growth rates at depths greater than a few mm could be measured. Four tests were run, three with synthetic seawater and one with saturated magnesium chloride brine. As shown in Figure 2.6-2 [*Shirai et al.* 2011, Figure 3-2], the seawater and magnesium chloride brine were applied as a single 20µL droplet in the center of the beam. *(It should be noted that in several conference publications, and in Figure 3-6 of the same CRIEPI project report, the salt was described as being applied as a spray, with a loading of 10 g/cm² Cl. This is inconsistent with the earlier Figure 3-2, and with the text in the report. Given the droplet loading scheme, and the fact that saturated magnesium chloride brine contains*

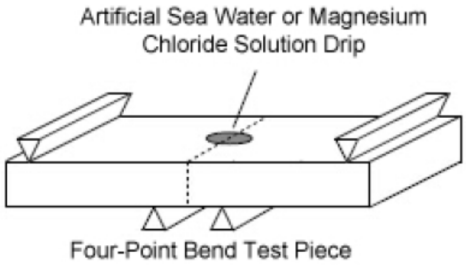

Figure 2.6-2. CRIEPI 4-point bend tests [*Shirai et al.* 2011; Figure 3-2].

15 times as much Cl as seawater, it seems clear that the actual salt loadings used for the bend tests varied, and are poorly defined). Crack areas were measured by DCPD, and depths were estimated by assuming a half-elliptical crack observed crack aspect ratio at the end of the experiment was typical of the entire experiment—that is, that the crack aspect ratio was constant. The observed a/c (crack depth to half length) ratios were between 0.5 and 1.

Observed crack depths over time are given in Figure 2.6-3 [*Shirai et al*. 2011a, Figure 3.6]. For each of the three samples loaded with synthetic seawater, the crack growth curves seem to show two segments. These is an initial fast growth, which transitions into a much slower, steady rate at a depth of about 2-3 mm. The early crack growth rate data that were measured ($\sim 4 \times 10^{-10}$ m s^{-1}) are consistent with the other studies presented here; but the long-term rate is much slower ($\sim 2 \times 10^{-11}$ m s^{-1} to 8×10^{-12} m s^{-1}). For the sample loaded with saturated magnesium chloride brine, there was no slowing of CGR with depth. The initial interpretation of the slowing in crack growth was that it was due to the changing stress state in the bend sample with depth (*Shirai et al*. 2011a); if so, then the slower rate would not be applicable to SNF storage canisters, which have been shown to have through-going tensile stresses. However, several other papers by CRIEPI make use of the slower rate data when assessing possible canister penetration rates without comment (e.g., *Tani et al.* 2010; *Shirai et al.* 2011b). *EPRI* [2014] makes use of the bimodal crack growth data and attributes the slower rate at depth to cathodic limitations related to the thin and discontinuous brine film and the presence of undissolved salt particulates; in the case of magnesium chloride, all salts would have deliquesced, so cathodic limitation would not occur.

It is important to note that the long-term CRIEPI rate does not represent the "plateau rate" that is commonly seen with increasing K_I, because the rate actually drops to a constant low value, rather than increasing to a constant maximum value.

Because of the potential importance of the CRIEPI observations, we discuss the experiments here in detail. There are many issues with interpreting or applying the CRIEPI data:

Use of DCPD to estimate elliptical crack depth requires assuming a constant crack aspect ratio.

CRIEPI utilized reversing DCPD to measure crack length as a function of time – little information is provided on the current used or the positioning of the voltage sense leads relative to the crack being measured. As demonstrated by CRIEPI, DCPD data only provided a voltage proportional to the area of the crack, not the crack geometry or instantaneous depth of the crack. Crack depths were estimated assuming a half-elliptical crack with a constant c/a ratio. The reported crack depths were calculated assuming a constant crack aspect ratio, although the ratio was not specified for each test. This assumption is most likely incorrect. *Newman and Raju* [1981] have shown that for fatigue crack growth under bending, no matter the starting a/c, the a/c will quickly follow the line where $a/c = 1 - (a/t)$, where t is sample thickness. This is because of variations in K_I along the perimeter of the crack, and the dependence of the CGR on K_I. It is not clear that this relationship is applicable to SCC, which also faces constraints related to reactant transport and possibly cathode area (see below), but if it is applicable to these bending tests, the a/c would start at 1 and decrease to 0.7 at 3 mm depth. Hence, calculated crack depths, which assume a constant aspect ratio, would be incorrect.

Application of salts as a droplet instead of as a uniform coating.

In the 4-point bend tests, salts were applied to the beam by placing a 20 µL droplet of either synthetic seawater or saturated $MgCl_2$ solution on the center of the beam. If deposited as a hemispherical droplet, this would correspond to a spot 4.2 mm in diameter; however, the droplet may have spread out to be larger. Because the salt was deposited as a droplet, the limited size of the salt-covered area may have artificially limited the external surface area of the sample that could act as a cathode. This would especially be true once the length of the crack extended beyond the edge of the droplet, and further growth would require diffusion along the crack to the crack tip outside of the salt covered area. For a crack aspect ratio of c/a =1, this would occur when the crack length exceeded 4-6 mm (corresponding to a

crack depth of 2.0-3.0 mm) exactly where the slow-down in growth occurred in the CRIEPI experiments. For a surface evenly coated with salts, the cathode would be adjacent to and surrounding the crack tip, where it intersects the surface. Why would the magnesium chloride specimen see no slowing of crack growth? Because at the temperature and RH used, the entire salt droplet would be deliquesced, and may have spread to cover a much larger fraction of the surface (or completely wetted the growing crack).

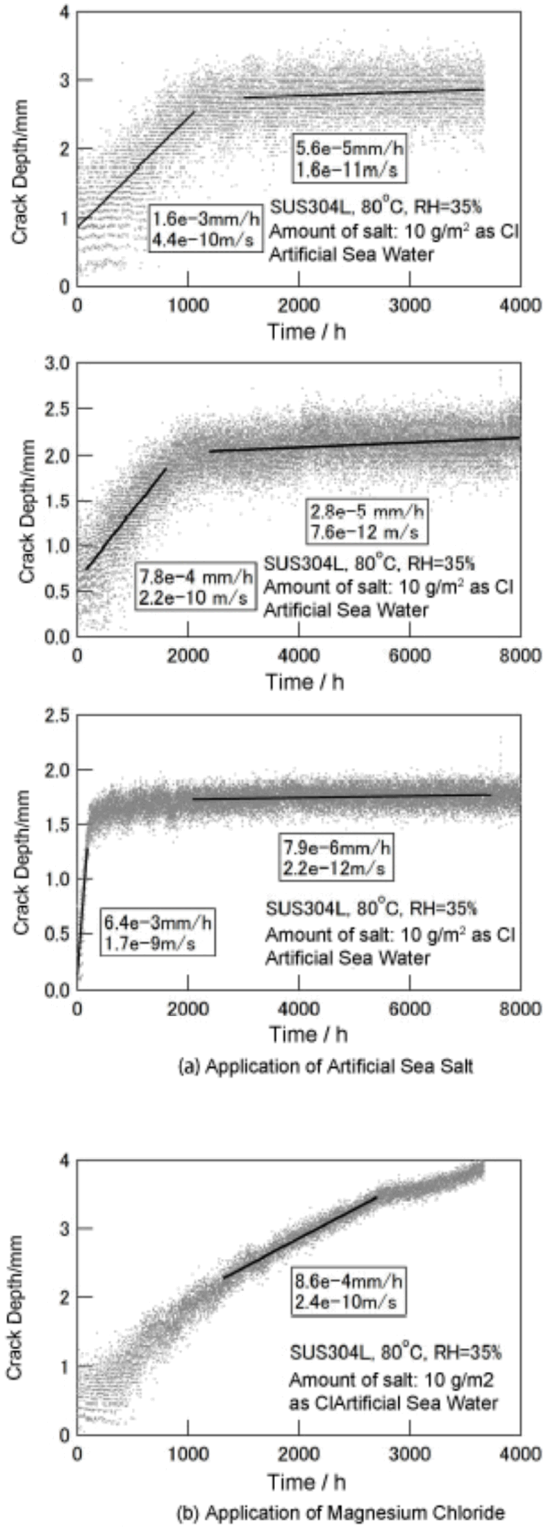

(a) Application of Artificial Sea Salt

(b) Application of Magnesium Chloride

Figure 2.6-3. Crack growth data collected by *Shirai et al.* [2011a].

Use of a bend specimen introduces a changing stress field with depth.

Four-point bend specimens are commonly used to assess susceptibility to stress corrosion cracking, and there is an ISO method for this: ISO/FDIS 16540 *Corrosion of metals and alloys — Methodology for determining the resistance of metals to stress corrosion cracking using the four-point bend method.* However, this method is for assessing SCC susceptibility, not for measuring crack growth rates. The reason for this is given in the ISO method:

> *The four-point bend test is a constant displacement test that is performed by supporting a beam specimen on two loading rollers (bearing cylinders) and applying a load through two other loading rollers so that one face of the specimen is in tension (and uniformly stressed between the inner rollers) and the other is in compression. The stress at mid-thickness is zero and there will be significant gradients in stress through the thickness, this being most marked for thin specimens. As a consequence, cracks may initiate, but then arrest or their growth rate decrease.*

In the four-point bend specimens used by CRIEPI, the initial bending moment produced a 270 MPa outer fiber tensile stress; which decreased to 0 at a neutral plane in the center of the sample. With further increases in depth, the stress state becomes increasingly compressive, finally reaching a value of 270 MPa compressive stress at the inner fiber of the sample. As a crack propagates though the sample, the change in stress condition is reflected in the crack tip stress intensity factor (K_I). Values of K_I as a function of crack depth at crack tip locations corresponding to the bottom of the crack (90º) and the crack tip at the surface (0º) been recalculated here (Figure 2.6-4) using the methods of *Newman and Raju* [1979]. Also shown is the predicted change in K_I for an infinite plate under the same bending moment, and the results are also shown for a crack in a sample under a uniform tension of 270 MPa, instead of under a bending moment. Uniform tension is a good representation for a storage canister, because even a through-penetrating SCC crack will be very small relative to the area of the outside of a storage canister (5 m long and about 5.3 m in circumference). All calculations were done using a crack depth to half-length ratio (a/c) of 1. That is, the crack is assumed to be semicircular (although CRIEPI reported a/c values of 0.5 to 1).

In the case of the infinite plate, if $a/c = 1$, then K_I at the bottom of the crack (90º) initially increases with depth, and then, after reaching a depth of a 1-2 millimeters, begins to decrease, passing though zero at a depth of 5 mm, or half the plate thickness. This is because, in an infinite plate, lateral constraints maintain the original stress profile in the sample. For a sample the dimensions of the CRIEPI beam, some constraint is lost as the crack grows and the crack length becomes a significant fraction of the beam width. This result is a downward shifting of the neutral plane below the crack, and the neutral plane is forced down to about 7.4 mm. At the 0ºC position, on the surface of the sample, K_I continues to increase as the crack grows. Thus, K_I varies greatly around with location on the crack tip, from the surface to the bottom. It is unlikely that this actually occurs—instead, the crack aspect ratio probably changes as the crack grows, maintaining a more or less constant K_I along the perimeter of the crack. For instance, for a longer, shallower crack ($a/c = 0.5$), K_I is nearly constant along the entire crack perimeter.

Conversely, in a sample under uniform tension (i.e., constant load), K_I continues to increase as the crack depth increases until penetration occurs. Moreover, the value of K_I varies only slightly with location on the crack tip, from where it intersects the surface to the bottom of the crack. Hence, the crack aspect ratio may remain more or less constant as the crack grows.

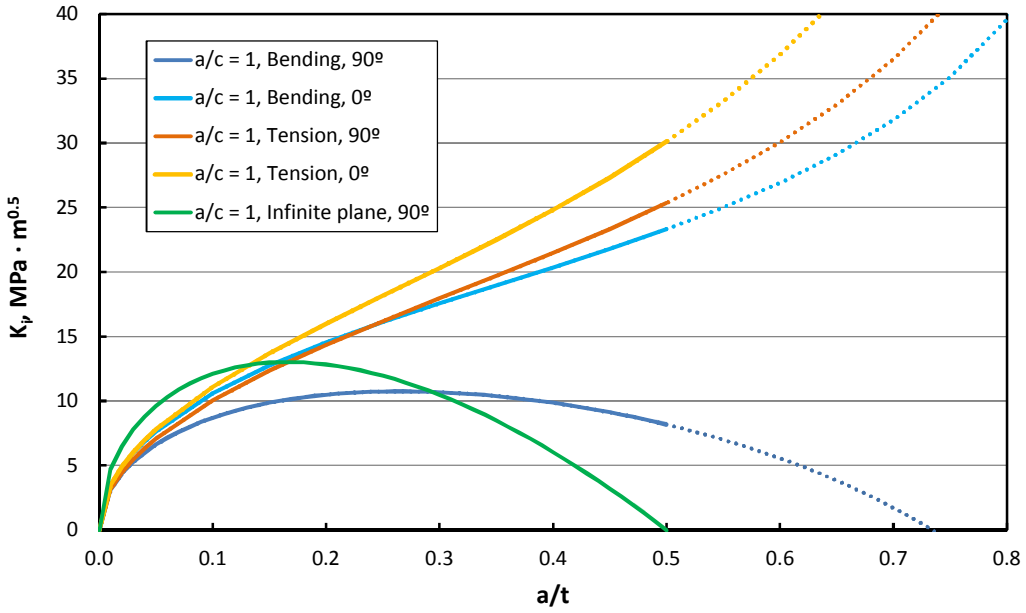

Figure 2.6-4. Stress distribution in the CRIEPI four-point bend specimens, calculated using the methods of *Newman and Raju* [1979]. Dotted lines are outside of the range of the model used to calculate K_I values.

One important aspect of this is that, in a bend specimen, the K_I varies strongly as a function of crack aspect ratio and of location along the advancing crack front, and that relationship changes with increasing crack depth. If we assume that crack growth tends to preserve a constant K_I along the crack tip, then the crack aspect ratio will change as the crack grows, just as it does for fatigue cracks. On the other hand, for a sample under uniform and constant tension, the difference in K_I along the crack front is much smaller, suggesting that the crack should be more semicircular ($a/c = 1$). This behavior has been observed experimentally and modeled theoretically for fatigue cracks by *Newman and Raju* [1981], and may apply to SCC cracks as well.

Again, why was the magnesium chloride specimen not affected? Possibly because the deliquesced droplet was larger, supporting more lateral crack growth—as the crack grows longer, the predicted stress distribution changes, and K_I no longer rolls over as in Figure 2.6-4, but instead continues to increase with depth.

Application of the CRIEPI model.

Even should the EPRI interpretation of cathodic limitation in the case of sea-salts be correct, it is important to note that the actual fraction of the salts in sea-salt that deliquesces is a function of RH. For a given salt load, at a higher RH, the brine volume increases dramatically. Crack growth rates may be more strongly controlled by deliquesced brine volume than by amount of salt present, the temperature, or the crack depth. An important part of any experimental study will be to isolate and evaluate each of these parameters individually.

2.7 Crack growth rates based on operational experience.

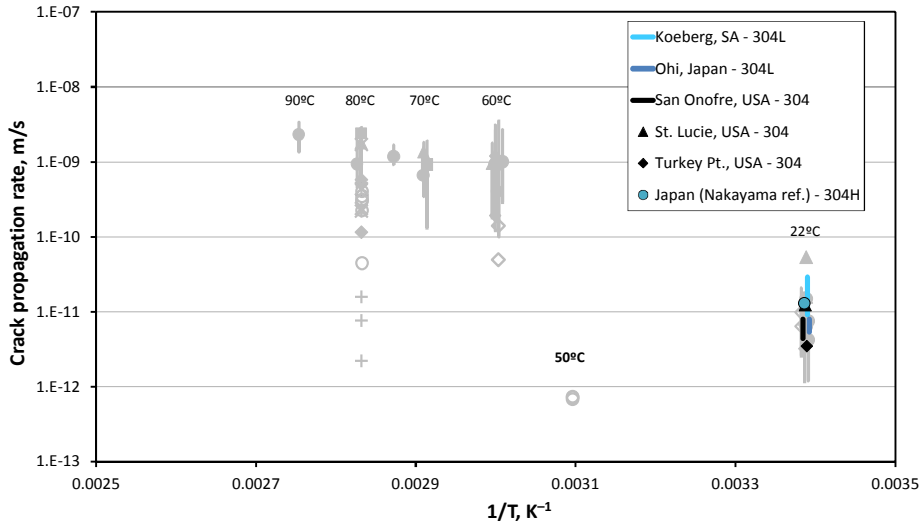

Figure 2.7-1. Data from nuclear plant operational experience.

While near-marine nuclear plants have frequently reported SCC of 304 SS, details are scarce. Estimates for crack growth rates from operating experience were recently summarized by the NRC [*Dunn*, 2015]. The data are all ambient temperature data, and are mostly for thinner components than SNF interim storage canisters. The available data shown in Table 2.7-1 [Dunn, 2015].

Table 2.7-1. Summary of reactor operating experience with atmospheric CISCC in welded stainless steel components [from *Dunn*, 2015]

Plant	Distance to salt water, m	Material and Component	Thickness, or crack depth, mm	Time in Service, years	Average crack growth rate, mm/yr
Koeberg (South Africa)	100	304L refueling water storage tank	5.0 to 15.5(?)[a]	17[b]	0.29 to 0.91(?)[a]
Ohi (Japan)	200	304L refueling water storage tank	1.5 to 7.5	30	0.17 to 0.25
St Lucie (FL, USA)	800	304 refueling water storage tank pipe	6.2	16	0.39
Turkey Point (FL, USA)	400	304 pipe	3.7	33	0.11
San Onofre (CA, USA)	150	304 pipe	3.4 to 6.2	25	0.14 to 0.25

[a]Cracks were observed in the thickest components, but it is not clear if penetration occurred.
[b]Some thin-walled components apparently failed within as little as 11 years, but details are unavailable.

The most extensive and perhaps best documented examples of atmospheric SCC due to marine salts are from the Koeberg Nuclear Power Station in South Africa. At this facility, several different 304L components of a borated water storage tank system and associated piping were degraded by externally-induced atmospheric stress corrosion cracking. On the storage tanks, SCC was most commonly observed in areas where attachment fillet welds and butt plate welds created high residual stresses. In the piping, SCC occurred due to high stresses imparted during pipe and elbow fabrication [*Alexander et al.*, 2010]. The water tanks in question are 16-17 meters high, and consist of 5 cylinders welded together, the lowermost being 15.5 mm thick and the uppermost, 5 mm thick. The tank roof is also 5 mm thick. All thicknesses exhibited SCC. The tanks are not pressurized, and the system was ambient temperature.

The plant began operation in 1984. The water storage tanks were originally constructed in the open, but were enclosed in specially-built rooms in 1990; although this reduced the rate of salt deposition by an estimated 2 orders of magnitude and the tanks were periodically washed, it has been speculated that enclosing the tanks exacerbated the SCC problem by eliminating rain-washing of salts from the surface of the tanks and piping [*Alexander et al.*, 2010; *Basson and Wicker*, 2002]. A few pinhole leaks near welds were identified as early as 1990, but were attributed to weld flaws. Several more leaks of thinner walled 304 SS components occurred between 1995 and 2001, when an extensive inspection program was initiated, and the extent of the problem was realized. Inspection of the piping and the tank indicated that the metal was extensively pitted, and that the pitted areas served as initiation points for SCC cracks. In a number of instances, while pitting was observed, no cracks were detected via dye penetrant – however, ultrasonic evaluation yielded indications. By grinding off 50-100 μm of metal from the surface, cracks were revealed and detected via dye penetrant examination. Cracks tended to initiate from the base of pits, and did not necessarily breach the metal surface, hindering detection without material removal via grinding. SCC cracks were present both as both linear cracks and networks. About 10% of all pipe spool pieces associated with one reactor were cracked, while a smaller number were cracked for the second reactor. Similarly, for one of the two water storage tanks examined, SCC cracks were associated with nearly all of the welds; the second tank was cracked to a lesser degree [*Basson and Wicker*, 2002].

CGR were not explicitly calculated, but have been estimated, based on installation and crack detection dates to be 0.29-0.91 mm/yr. These would be minimum crack growth rates, as no incubation time was assumed.

Nakayama and Sakakibara [2013] describe an additional example of atmospheric SCC of a large diameter 304 (0.079% C) pipe at a Japanese nuclear plant. The crack initiated externally and occurred where there had been a weld repair on the internal surface of the pipe, further sensitizing the material in the weld heat affected zone. The pipe was exposed to the atmosphere, and was found to typically have a NaCl surface load of 0.1 g/m^2; occasional rains washed the surface and prevented heavy buildup. The crack was confirmed to have penetrated about 14 mm in 35 years, or 0.4 mm/yr (1.3E-11 m/s). This is a minimum penetration rate, as the timing of crack initiation is not known, nor was it known exactly when penetration occurred.

2.8 Crack growth rate data collected under immersed conditions, for high chloride brines

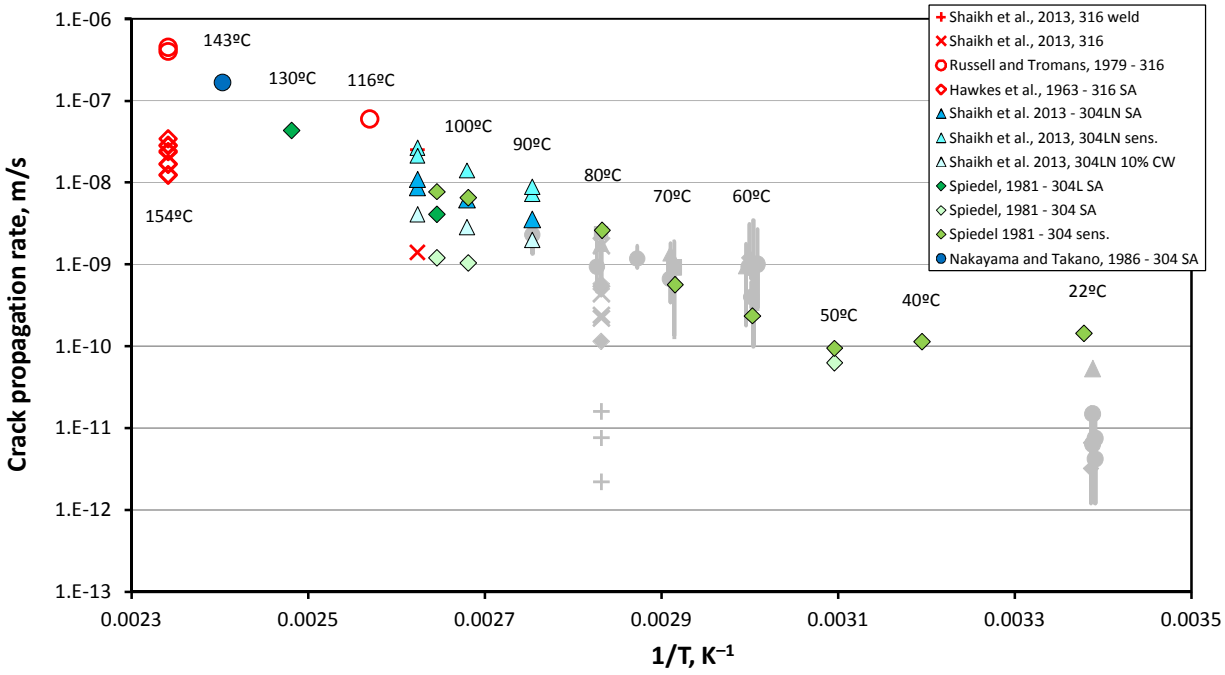

Figure 2.8-1. Data from chloride-rich brine immersed experiments.

Data for SCC crack growth rates under immersed conditions in chloride-rich brines have been compiled and are provided here as a potential talking point. The data extend to higher temperatures than data collected for atmospheric SCC. An aqueous brine cannot be present at temperatures higher than 60-70ºC, based on the possible range of absolute humidities in air circulating through a SNF interim storage system; however, these data may provide insights into the mechanism of the corrosion process.

The following data sets have been identified:

- *Spiedel* [1981] — Solution annealed 304L, in 42% $MgCl_2$ (130ºC), and in 22% NaCl (105ºC). Also, solution annealed and sensitized 304 samples, in 22% NaCl, over a range of temperatures from 23ºC to 105ºC.
- *Shaikh et al.,* [2013] — 316LN base and weld metal samples, in 5M NaCl + 0.15 M Na_2SO_4 + 2.5 ml/L HCl. Also, solution annealed, sensitized, or 10% cold worked 304LN samples, at 90ºC, 100ºC, and 108ºC, in the same solution.
- *Russell and Tromans*, [1979] — Cold worked (25 and 50%) 316 SS in 44.7% $MgCl_2$, at 116 and 154ºC.
- *Hawkes et al.*, [1963]. — Solution annealed 316 SS in 42% $MgCl_2$, at 154ºC.
- *Nakayama and Takano*, [1986]. — Solution annealed 304 SS, in 42% $MgCl_2$, at 143ºC.

2.9 Summary

Available SCC crack growth rate data from corrosion testing under atmospheric conditions is highly scattered, in part due to wide variety of testing methods used to collect the data. Other contributing factors are study-to-study variations in potentially important parameters such as salt load and RH. Moreover, operational experience from operating reactors does little to fill the knowledge gaps, as it is restricted to ambient conditions. While ambient testing and operational experience yield relatively similar SCC crack growth rates, the potential effects of temperature are poorly understood. Corrosion is a thermally activated process, and under immersed conditions, CGR increases with temperature. However, under atmospheric conditions, elevated temperatures correspond to lower relative humidity (RH) values, which in turn result in (1) more concentrated, potentially more corrosive brines, and (2) smaller brine volumes (thinner brine films for a given salt load) which may limit the size of the cathode area on the metal surface, or limit transport between the anode and cathode. Sufficient data do not appear to be available to currently predict what the effects of elevated surface temperatures on SCC crack initiation or growth under a deliquesced brine film.

3. References

Alexander, D., P. Doubell, and C. Wicker (2010), Degradation of Safety Injection System and Containment Spray Piping and Tank Fracture Toughness Analysis, *FONTEVRAUD 7, Contribution of Materials Investigations to Improve the Safety and Performance of LWRs*, 26-30.

Basson, J., and C. Wicker (2002), Environmentally induced transgranular stress corrosion cracking of 304L stainless steel components at Koeberg, *Proc. Fontevraud*, *5*.

Cook, A., N. Stevens, J. Duff, A. Mishelia, T. S. Leung, S. Lyon, J. Marrow, W. Ganther, and I. Cole (2011), Atmospheric-induced stress corrosion cracking of austenitic stainless steels under limited chloride supply, *Proc. 18th Int. Corros. Cong., Perth, Australia*.

Dunn, D. S. (2015), NRC Perspective on Information Needs for CISCC of Spent Fuel Dry Storage Systems, in *DOE UFD Stress Corrosion Cracking Workshop, 22 Sept. 2015*, edited, Las Vegas, NV.

EPRI (2014), Flaw Growth and Flaw Tolerance Assessment for Dry Cask Storage Canisters*Rep. 3002002785*, 84 pp, Electric Power Research Institute, Palo Alto, CA.

Hawkes, H., F. Beck, and M. Fontana (1963), Effect of Applied Stress and Cold Work On Stress Corrosion Cracking of Austenitic Stainless Steel By Boiling 42 Percent Magnesium Chloride, *Corrosion*, *19*(7), 247t-253t.

Hayashibara, H., M. Mayuzumi, and Y. Mizutani (2008), Effects of temperature and humidity on atmospheric stress corrosion cracking of 304 stainless steel, *CORROSION 2008*.

Kosaki, A. (2008), Evaluation method of corrosion lifetime of conventional stainless steel canister under oceanic air environment, *Nuclear Engineering and Design*, *238*(5), 1233-1240.

Lu, B., Z. Chen, J. Luo, B. Patchett, and Z. Xu (2005), Pitting and stress corrosion cracking behavior in welded austenitic stainless steel, *Electrochimica Acta*, *50*(6), 1391-1403.

Nakayama, G., and Y. Sakakibara (2013), Prediction Model for Atmospheric Stress Corrosion Cracking of Stainless Steel, *ECS Transactions*, *50*(31), 303-311.

Nakayama, T., and M. Takano (1986), Application of a slip dissolution-repassivation model for stress corrosion cracking of AISI 304 stainless steel in a boiling 42% MgCl2 solution, *Corrosion*, *42*(1), 10-15.

Newman, J., and I. Raju (1981), An empirical stress-intensity factor equation for the surface crack, *Engineering Fracture Mechanics*, *15*(1), 185-192.

Newman, J. C., and I. S. Raju (1979), Analysis of Surface Cracks in Finite Plates Under Tension or Bending Loads*Rep.*, NASA, Hampton, VA.

Russell, A. J., and D. Tromans (1979), A fracture mechanics study of stress corrosion cracking of type-316 austenitic steel, *Metallurgical Transactions A*, *10*(9), 1229-1238.

Shaikh, H., H. Khatak, and P. Rodriguez (2013), Stress corrosion crack growth behaviour of austenitic stainless steels in hot concentrated chloride solution, paper presented at ICF10, Honolulu (USA) 2001.

Shirai, K., J. Tani, and T. Saegusa (2011a), Study on Interim Storage of Spent Nuclear Fuel by Concrete Cask for Practical Use -- Feasiblity Study on Prevention of Chloride Induced Stress Corrosion Cracking for Type 304 Stainless Steel Canister (English translation) *Rep.*

Shirai, K., J. Tani, M. Wataru, T. Saegusa, and C. Ito (2011b), Long-term containment performance of test metal cask. 10-14 April, in *International High-Level Radioactive Waste Managment Conference (IHLRWMC)*, edited, pp. 816-823, American Nuclear Society, Albuquerque, NM.

Shirai, K., J. Tani, T. Arai, M. Wataru, H. Takeda, and T. Saegusa (2011c), SCC evaluation test of a multi-purpose canister. 10-14 April, paper presented at 13th International High-Level Radioactive Waste Management Conference (IHLRWMC), American Nuclear Society, Albuquerque, NM.

Speidel, M. O. (1981), Stress corrosion cracking of stainless steels in NaCl solutions, *Metallurgical Transactions A*, *12*(5), 779-789.

Spencer, D., M. Edwards, M. Wenman, C. Tsitsios, G. Scatigno, and P. Chard-Tuckey (2014), The initiation and propagation of chloride-induced transgranular stress-corrosion cracking (TGSCC) of 304L austenitic stainless steel under atmospheric conditions, *Corrosion Science*, *88*, 76-88.

Tani, J. I., M. Mayuzurmi, and N. Hara (2009), Initiation and propagation of stress corrosion cracking of stainless steel canister for concrete cask storage of spent nuclear fuel, *Corrosion*, *65*(3), 187-194.

Tani, J. I., K. Shirai, M. Wataru, and T. Saegusa (2010), Stress Corrosion Cracking of Stainless Steel Canister of Concrete Cask, paper presented at International Seminar on Interim Storage of Spent Fuel (ISSF) 2010.

Yajima, M., and M. Arii (1980), Chloride Stress Corrosion Cracking of AISI 304 Stainless Steel in Air, *Materials Performance*, *19*(12), 17-19.